

ENabling Optimized DISruptivE airframe-propulsion integration concepts

H2020 Research and Innovation Action
Grant Agreement No 860103

Deliverable Reference Number: D4.5

Deliverable Title:
WP4 Final Public Report

Lead participant: DLR
Contributing participant(s): DLR, GPUP, ONERA, UR3, SISW, VKI, RWTH, ECL

10 November 2023

Start date of project: 1st of June 2020
Duration: 48 months

Type		
R	Document, report	X
DEM	Demonstrator, pilot, prototype, etc.	
DEC	Websites, patent fillings, videos, etc.	
ORDP	Open Research Data Pilot	
Dissemination Level		
PU	Public	X
CO	Confidential, only for members of the consortium (incl. Commission Services)	

APPROVAL

Title	Issue	Revision
WP4 Final Public Report	1	0

Author(s)	Date
S. Guérin, A. Falsi, S. Karabasov, H. A. Abid, M. Darouk, P. Clement, G. Reboul, S. Meloni, S. Le Bras, A. Zarri, Z. Yang, D. Acevedo Giraldo, M. Roger	10/11/2023

Approved by	Date
Christophe Schram	10/11/2023

Contents

1 Introduction **5**

2 Summary of the results obtained for the configurations A: wall-mounted and buried propulsion systems **5**

2.1 DLR contribution to configurations A1 and A2 . . . 5
2.1.1 Context and objectives . . . 5
2.1.2 Main achievements . . . 5
2.1.3 Lessons learned . . . 6
2.1.4 Dissemination (Publications + link ZENODO) . . . 7
2.2 Second DLR contribution to configurations A1 . . . 7

3 Results Dissemination **8**

3.1 GPUP contribution to configurations A1 and A2 . . . 8
3.1.1 Context and objectives . . . 8
3.1.2 Main achievements . . . 8
3.1.3 Lessons learned . . . 9
3.1.4 Dissemination (Publications + link ZENODO) . . . 9
3.2 ONERA contribution to configuration A1 with static blades . . . 9
3.2.1 Dissemination (Publications + link ZENODO) . . . 11
3.3 ONERA contribution to configuration A2-ducted . . . 11
3.3.1 Introduction . . . 11
3.3.2 Context and objectives . . . 11
3.3.3 Main achievements . . . 11
3.3.4 Lessons learnt . . . 12
3.3.5 Dissemination . . . 12
3.4 UR3 contribution to configuration A1 . . . 12
3.4.1 Context and objectives . . . 12
3.4.2 Main achievements . . . 12
3.4.3 Dissemination (Publications + link ZENODO) . . . 12

4 Summary of the results obtained for the configurations B: distributed pylon- and control surface-mounted propulsion systems **13**

4.1 VKI contribution to configuration B1 . . . 13
4.1.1 Context and objectives . . . 13
4.1.2 Main achievements . . . 13
4.1.3 Lessons learned . . . 13
4.1.4 Dissemination (Publications + link ZENODO) . . . 13
4.2 SISW contribution to configuration B1 . . . 14
4.2.1 Main achievements . . . 14
4.2.2 Lessons learnt . . . 14
4.2.3 Dissemination . . . 14
4.3 ONERA contribution to configuration B1 . . . 15
4.3.1 Context and objectives . . . 15
4.3.2 Main achievements . . . 15
4.3.3 Lessons learnt . . . 15
4.3.4 Dissemination . . . 15

4.4 DLR contribution to configurations B1 . . . 15
4.4.1 Context and objectives . . . 15
4.4.2 Main achievements . . . 15
4.4.3 Lessons learned . . . 16
4.4.4 Dissemination (Publications + link ZENODO) . . . 17
4.5 RWTH contribution to configuration B1 . . . 17
4.5.1 Context and objectives . . . 17
4.5.2 Main achievements . . . 17
4.5.3 Lessons learned . . . 18
4.5.4 Dissemination . . . 18
4.6 ECL contribution to configuration B2 . . . 19
4.6.1 Context and objectives . . . 19
4.6.2 Main achievements . . . 19
4.6.3 Lessons learned . . . 19
4.6.4 Dissemination (Publications + link ZENODO) . . . 20
4.7 ONERA contribution to configuration B2 - Auralization . . . 20
4.7.1 Context and objectives . . . 20
4.7.2 Main achievements . . . 20
4.7.3 Lessons learnt . . . 21
4.7.4 Dissemination . . . 21

5 Summary of the results obtained for the configurations C: multi-rotor propulsion systems 22
5.1 VKI & SISW contribution to configuration C . . . 22
5.1.1 Context and objectives . . . 22
5.1.2 Main achievements . . . 22
5.1.3 Lessons learned . . . 22
5.1.4 Dissemination (Publications + link ZENODO) . . . 23
5.2 ECL contribution to configuration C . . . 23
5.2.1 Context and objectives . . . 23
5.2.2 Main achievements . . . 23
5.2.3 Lessons learned . . . 24
5.2.4 Dissemination (Publications + link ZENODO) . . . 24
5.3 ONERA contribution to configuration C . . . 24
5.3.1 Context and objectives . . . 24
5.3.2 Main achievements . . . 24
5.3.3 Lessons learnt . . . 25
5.3.4 Dissemination . . . 25

6 Conclusion 26

1 Introduction

The report is divided in three main parts presenting an overview of the results of Work Package 4 obtained for the configurations A, B and C investigated in ENODISE. A summary of each partner's contribution is presented per task.

ENODISE deals with air vehicles for intracity and regional transport in first place. Distributed Electric Propulsion offers many possibilities in terms of vehicle architecture and integration of the propulsion system, often at the expense of greater interaction of the propulsion units and the airframe.

In ENODISE, several generic configurations are investigated based on low-TRL experiments with low Reynolds number and low Mach number.

Configuration A corresponds to a single two-bladed propeller partially immersed up to 44% in a boundary layer developing over either a (A1) flat plate or (A2) a curved surface. The configuration A2 was also investigated using a shrouded propeller. The measurements from the two different open-jet wind tunnels of Bristol University and Twente University were used for validation.

Configuration B aims at investigating the interaction of multi-propellers with a lifting surface. In configuration B1, three propellers with 6 blades are placed in front of a wing in the puller configuration, while the propellers are placed above the wing in configuration B2. For configuration B1, the validation data came from TU Delft, while for B2, ECL provided the measurement data.

Configuration C deals with the noise radiated by two-bladed contra-rotating propellers placed in tandem with and without shroud. The validation data came from VKI.

2 Summary of the results obtained for the configurations A: wall-mounted and buried propulsion systems

2.1 DLR contribution to configurations A1 and A2

2.1.1 Context and objectives

Beside experiments and numerical simulations demanding in computation resources, there is a need for simplified methods, which can capture the main physical effects at low to moderate computation cost, and therefore, are suited for pre-design study. The objective of DLR was to apply the modelling approach developed in the past for the AIAA FC3 benchmark case of Virginia Tech to the new configuration investigated in ENODISE. Both setups are similar but differ with respect to the rotor solidity and the number of the rotor blades. The simulation were done with the pre-design simulation program PropNoise, which is based on the acoustic analogy.

2.1.2 Main achievements

At first the emission of acoustic tones was investigated. The blade element momentum theory was applied to calculate the mean flow and the blade lift. The laminar–turbulent transition was considered in the process through the used of the flow solver XFOIL. The steady and unsteady loading mechanisms due to blade loading and rotor interaction with the boundary-layer velocity deficit, respectively, were modelled separately and superimposed linearly. The acoustic reflections by the plate were modelled with the method of image. The prediction results were in satisfactory agreement with the measurements (see example in Figure 1), in particular, they confirmed the growing contribution of BLI tones as the harmonic index of the blade passing frequency increases.

At second, the broadband noise generated by the BL turbulence hitting the propeller blades was predicted. The aero-acoustic model accounted for the fact that vortices could be chopped several times by the blades as they passed through the propeller. The "cigar" shape of the turbulence near the wall surface was considered in the turbulence model. If possible, the input parameters were retrieved from the hot-wire measurements, which had been carried out in the boundary layer, otherwise they were modelled. The effect of the flat plate on aerodynamics and acoustics was ignored for that part of the work. The results obtained with this heuristic approach were satisfactory in the orthogonal plane but the levels were underestimated by more than 10 dB in the downstream region of the horizontal plane as can be seen in

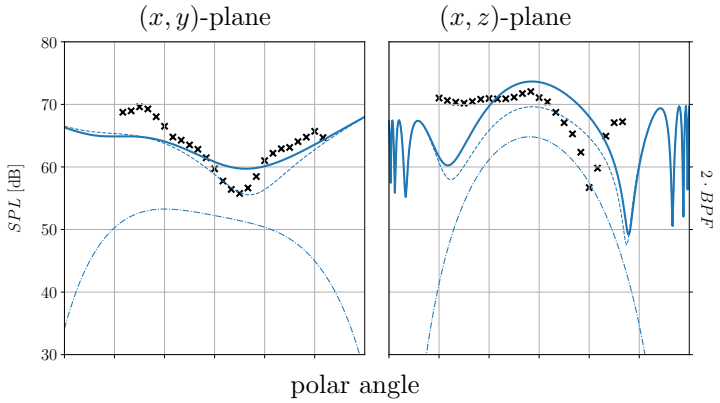

Figure 1: DLR results with BLI at 2BPF: (x) Bristol experimental data, (dotted-dashed line) sum of steady-lift and thickness noise, (dashed line) BL-rotor interaction, (thick line) total; polar directivity (left) perpendicular and (right) in the plane of the plate.

Figure 2. This suggests that a major effect was not captured by the current models. Measurements and predictions agreed upon the fact that blade-to-blade correlations were not prominent for this operating condition.

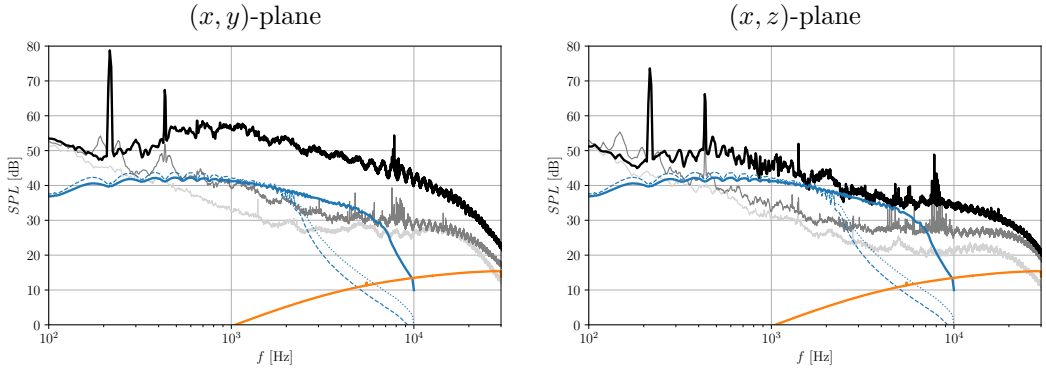

Figure 2: DLR results: Comparison between pressure spectra measured at U-BRI and predictions at downstream position $\psi = 50°$; experiments: (black) immersed propeller, (grey) isolated propeller without plate, (light gray) background noise of the set-up; predictions: (solid blue line) TBL–rotor interaction with $\max(k) = 30$, (dotted blue line) $\max(k) = 10$, (dashed blue line) $\max(k) = 10$ combined with length scales from Karve, (orange) trailing-edge noise.

2.1.3 Lessons learned

The comparison of the prediction with the measurements suggests that the DLR analytical approach, which only accounts for the gust–airfoil interaction mechanism, enables to capture some of the acoustic effects resulting from the boundary-layer ingestion. However, this conclusion is only valid for one operating condition near the peak efficiency. Other experimental results analysed by the University Roma Tre show that the sharp peaks centred on the BPF strongly broaden at low advance ratio. It remains to be investigated whether this effect can be captured with the current method.

This work has also highlighted the need for further development of the models in order, for example, to take better account of the concentration of turbulence near the wall and the acoustic reflections by the plate. The consistency between the various models chosen to describe the turbulence should be improved too.

2.1.4 Dissemination (Publications + link ZENODO)

The results regarding the prediction of tonal and broadband noise were presented separately at two international conferences [1, 2], in Prague (Czech Republic) and in Tokyo (Japan), respectively.

These data were uploaded on Zenodo repository and can be accessed using this link: `https://zenodo.org/record/8074991`.

2.2 Second DLR contribution to configurations A1

The second contribution of DLR AS-TEA to this report is the advancement in the simulations' activities concerning configuration A1. The results of the in-house mid-fidelity approach developed using the TAU/PIANO-IBC DLR's solvers to investigate rotor installation effects were compared with the datasets for the aeroacoustic experiments conducted at the University of Bristol [3]. The aerodynamic flow field was simulated with an Actuator Disc (AD) RANS approach, in which the AD replaces the propeller blades' geometry. The TAU AD model requires aerodynamic input data in tabular form for lift, drag, chord and twist angle distribution of different propeller blade sections. This input is necessary to determine the loads on the AD using a Blade Element Momentum (BEM) model. The lift and drag distribution of the 12 blade sections were computed using XFOIL. The computational domain for the RANS simulation includes the geometrically resolved experimental tripping device (trip C) used to achieve distinct thicknesses of the boundary layer at the propeller location.

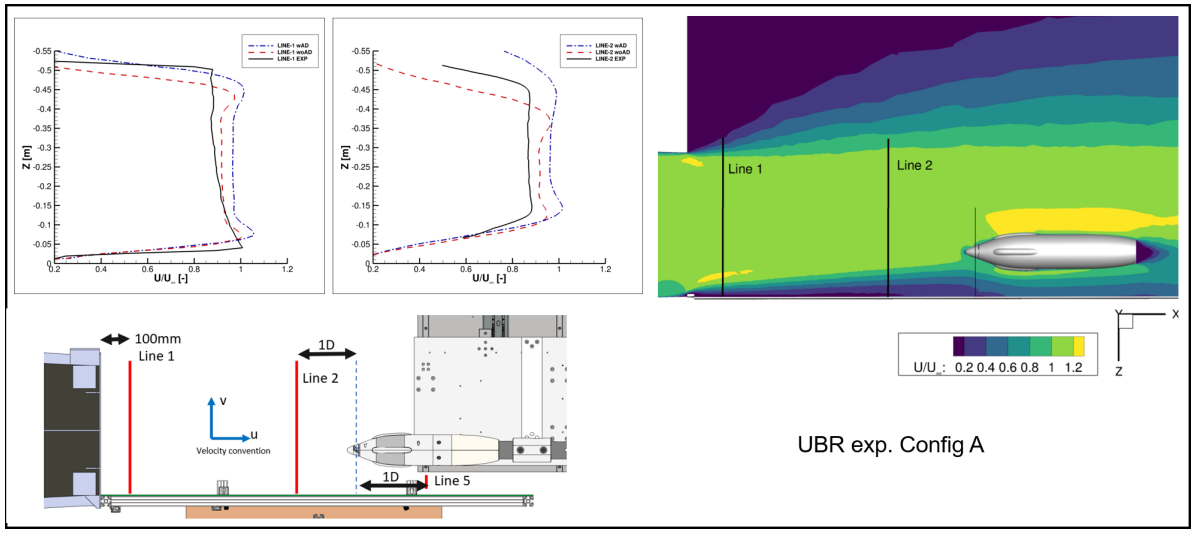

Figure 3: Results of the AD-RANS simulation, including a comparison with available experimental data. In the plots legend, wAD and woAD refer to simulations of the complete configuration with and without the AD, respectively.

A hybrid structured-unstructured mesh was generated, for a total of 15 million mesh points. The mesh resolution close to solid-wall surfaces satisfies the $y^(+) = 1$ condition $(= 7.28810^(-6)m)$ in the wall normal direction. On the nacelle, pylon, nacelle support sting, and hub surface, a no-slip wall boundary condition is applied. A pressure-inflow boundary is specified at the nozzle inlet, while the opposite domain surface in the farfield is prescribed a pressure-outflow boundary condition. This is necessary for a close agreement of simulations with experiments. The turbulence model used is the k-Omega SST model of Menter. Additional parameters of the configuration investigated can be found in Fig. 4. Figure 3 shows a good agreement between simulatively predicted and experimental results. For the CAA simulations, the octree-hierarchical 4th order dispersion-and-dissipation-optimised computational aeroacoustics (CAA) PIANO solver of DLR was used. The grid generated consists of a rectangular domain $(7.9x5.0x3.8[m])$, for a total of 32 million grid mesh points. The maximum resolved frequency is $3kHz$. An immersed/embedded boundary method is used for the hub, nacelle, pylon, and support

sting. Hanging nodes at inner boundaries are used to impose a no-slip wall boundary condition for the above solid surfaces. At the far-field boundaries, a radiation boundary condition, in combination with a sponge layer and an outflow boundary condition in downstream direction for the outgoing slipstream are imposed. Virtual microphones are located at a distance of $4R$ and $z/R = 0$, in a circular arrangement. Figure 5 shows the initial results obtained for the CAA predition model, which highlights the different propagation patterns for the installed configuration, compared to an equivalent simulated isolated rotor.

RANS AD (k-ω Menter SST)	EXP (UBR)
Ω = 6500 RPM	Ω = 6500 RPM
BPF = 108.333 Hz	BPF = 108.333 Hz
J = 1 [-]	J = 1 [-]
U_∞ = 33 m/s	U_∞ = 33 m/s
T_{ad} = 10.606 N	T_{prop} = 10.198 N
Q_{ad} = -0.625 N.M	Q_{prop} = -0.605 N.M
C_{T_ad} = 0.08496 [-]	C_{T_prop} = 0.08165 [-]
MF_{inlet} = 16.082 kg/s	-
MF_{ad} = 2.884 kg/s	-
Tip clearance t = 5 mm (1/30 R)	Tip clearance t = 5 mm (1/30 R)
Trip C : 25 x 10 mm (W x H)	Trip C : 25 x 10 mm (W x H)

Figure 4: Simulation Parameters

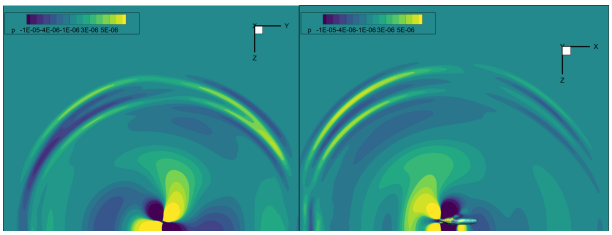

Figure 5: Contour plot of p'. Left, equivalent isolated propeller, right installed propeller (A1 config.)

3 Results Dissemination

Seyed Mohsen Alavi Moghadam, Jürgen Dierke, Michael Moessner, Roland Ewert and Jan Delfs. "A mid-to-high fidelity aerodynamic noise simulation framework for installed propeller configurations," AIAA 2022-3007. 28th AIAA/CEAS Aeroacoustics 2022 Conference. June 2022.

Andrea Franco , Seyed Mohsen Alavi Moghadam, Michael Mößner, Jürgen Dierke, Roland Ewert and Jan Werner Delfs, "Fast Non-Empiric Rotor Noise Prediction Model for Installed Propulsors," Aeroacoustic Installation Effects in Conventional and New Aircraft Propulsion Systems, DJINN-ENODISE conference, 22-24 November 2023, Berlin (To be presented)

3.1 GPUP contribution to configurations A1 and A2

3.1.1 Context and objectives

The GPUP contribution in this task is to apply high-fidelity Navier-Stokes flow solutions (Wall Modelled Large Eddy Simulations) based on the high-resolution CABARET scheme on rotating meshes (developed in Work Package 2) coupled with a penetrable Ffowcs Williams – Hawkings (FW-H) acoustic integration method for boundary layer ingestion/installed propeller noise problems. Two benchmark problems considered for validation correspond to a generic two-bladed propeller installed in a thick boundary layer close to a flat plate and an S-shape adverse-boundary layer surface (configurations A1 and A2). The corresponding experimental flow and noise data were provided by the University of the Bristol for validation.

3.1.2 Main achievements

The dataset for configuration A1 corresponds to a rotational frequency of the rotor at 6500RPM and a free-stream velocity of Uinf=33m/s. In this case, comparisons of the meanflow axial velocity profiles with the hotwire data are provided at an upstream (x=1Db) and a downstream location (x=-1Db), where the rotor plane corresponds to x=0. Noise spectra results are provided for polar angles at 60, 90, and 120 degrees with respect to the upstream propeller axis. The acoustic results are obtained for both the overhead and sideline arrays. The A2 dataset corresponds to the same rotational frequency of the rotor as for configuration A1 (6500RPM) and a free-stream velocity of Uinf=27m/s. In this case, comparisons of the meanflow lateral velocity profiles with the hotwire data are provided at just one upstream location

(x=-280mm measured from the rotor plane). In each A1 and A2 configuration case, an effective non-uniform inflow condition upstream of the rotor is imposed so that the velocity distribution at a target location upstream of the rotor matches the experiment. A locally refined mesh is used to capture the most critical regions such as around the propeller blade tips and the boundary layer, thereby capturing major low/mid-frequency rotor blade/ wake interaction effects. The numerical simulations are executed for a total of 30 rotor revolutions, and the statistical averaging is applied for the data time history collected between the 10th to the 30th revolutions to avoid initial transients. For far-field noise modelling with the FW-H method, multiple penetrable surfaces are used confining the rotor and a downstream wake region. The far field signals obtained from each FW-H surface are averaged in order to eliminate the spurious noise generated by vorticity wave crossing the surfaces. The noise spectra predictions show encouraging agreement with the experiment in capturing the main low-frequency tones and the broadband part of the spectra for mid-range frequencies.

3.1.3 Lessons learned

To improve the current coarse grid results, a refinement of the grid resolution is required, which would allow to capture the turbulent wake effects as well as properly represent the adverse pressure gradient flow for Configuration A2. Furthermore, an improved acoustically quiet synthetic turbulent inflow boundary condition is needed as well as a more accurate ensemble averaging technique to better resolve low frequency tones in the acoustic spectra whilst reducing numerical noise at high-frequencies.

3.1.4 Dissemination (Publications + link ZENODO)

The resulting datasets are uploaded on Zenodo repository and can be accessed using `https://zenodo.org/record/8227807` for configuration A1 and `https://zenodo.org/record/8306579` for configuration A2. For both configurations, the uploaded datasets are divided into the comparison of time-averaged flow velocity ('hotwire dataset') and the far field noise spectra ('acoustic dataset').

3.2 ONERA contribution to configuration A1 with static blades

In this task, a numerical simulation of configuration A1 is performed. The aim of this simulation is to investigate the interaction between a thick turbulent boundary layer and a fixed blade. More particularly, the effect of the large-scale structures of the boundary layer on the broadband noise radiation is addressed.

The flow conditions and geometries of UTWE have been retained for the study. Only the case with the fixed (*i.e.* non-rotating) propeller is considered, for a vertical position of the propeller. The inflow velocity is $U_\infty = 30$ m/s and the propeller diameter is $D = 0.3048$ m.

The targeted boundary layer thickness at the propeller location ($x = 0$) is the thickest one ($\delta_{x=0} \simeq 0.15$ m) that was obtained in the UTWE experiments. Reaching this boundary layer thickness using a scale-resolving approach on a limited computational domain represents one of the main challenges of this study. The numerical methodology relies on the following ingredients:

1. **Turbulence modeling and numerical method:**
   The numerical method retained for this study is the scale-resolving approach developed in Task 2.4. It relies on the coupling between a hybrid RANS/LES approach (ZDES mode 3 [4, 5]) and a wall model, on a set of octree Cartesian grids with immersed boundary conditions. It yields a significant reduction of the near-wall grid resolution requirements, while allowing for an explicit resolution of the turbulent scales in the outer region of the boundary layer. The adaptations of the ZDES solver to perform such simulations (wall model and tripping strategy at the inflow) are fully documented in the deliverable D2.9 [6]. In order to investigate the effect of the resolved turbulent scales on the boundary layer interaction with the propeller, a second simulation based on the ZDES mode 2 (2020) [7] has also been carried out. In this case, the whole boundary layer is resolved in RANS mode, with no explicit resolution of the outer layer turbulent structures.

2. **Computational domain and boundary conditions**
   The computational domain extends over a distance of 6.4m× 1m× 3m in the respective streamwise,

spanwise and vertical directions, with about 5m of flat plate located upstream of the propeller plane. The overall number of grid points required for the simulation is about 500 millions, with a near-wall grid resolution of about 50 wall units all along the flat plate and a finer grid resolution $\Delta x = 0.38$ mm close to the propeller. Specific boundary conditions have been developed for the test case. Except at the wall, non-reflective characteristic boundary conditions are used, where the reference inflow/lateral/outflow condition is given by an analytical boundary layer profile. This profile is based on the SA wall law [8], combined with a wake correction [9]. It depends on the local theoretical values of the boundary layer thickness $\delta(x) \simeq 0.16 x Re_x^{-\frac{1}{7}}$ and skin friction coefficient $C_f \simeq 0.058 Re_x^{-1/5}$.

3. **Boundary layer tripping:**
   For the ZDES mode 3 simulation, an artificial tripping of the boundary layer is required, in order to trigger the development of resolved turbulent structures in the outer region of the boundary layer. For that purpose, a specific treatment based on the introduction of small vertical rods near the wall at the inflow of the domain has been retained, as detailed in the deliverable D2.9 [6]. The precise size and spacing of these rods has been chosen such that they trigger some of the most unstable modes of the boundary layer, (height of the rods $h = 0.3\delta_0$ and spanwise spacing of the rods $\lambda = 0.5\delta_0$).

The results are fully detailed in Deliverable 4.4. For illustration, Figure 6 presents instantaneous visualizations of the flow for the respective ZDES mode 2 and mode 3 simulations. For the ZDES mode 3 simulation, it is clear that the introduction of the roughness elements at the inflow of the domain is really efficient to trigger quickly the generation of realistic turbulent scales in the boundary layer, in a silent way. The classical topology of a fully-developed turbulent boundary layer is recovered, with typical hairpin-like vortices (see Figure 6, right). The interaction between the large-scale structures of the boundary layer and the propeller's lower blade is clearly visible for the ZDES mode 3 computation. Some differences are also visible for the radiated acoustic field, which appears to be "cleaner" when the boundary layer structures are explicitly resolved. A possible scenario for this counter-intuitive phenomena may that the tonal character of the noise source at the lower blade is lowered in this case, thus lowering its interference with the tonal noise source at the upper blade. This will however require further investigations.

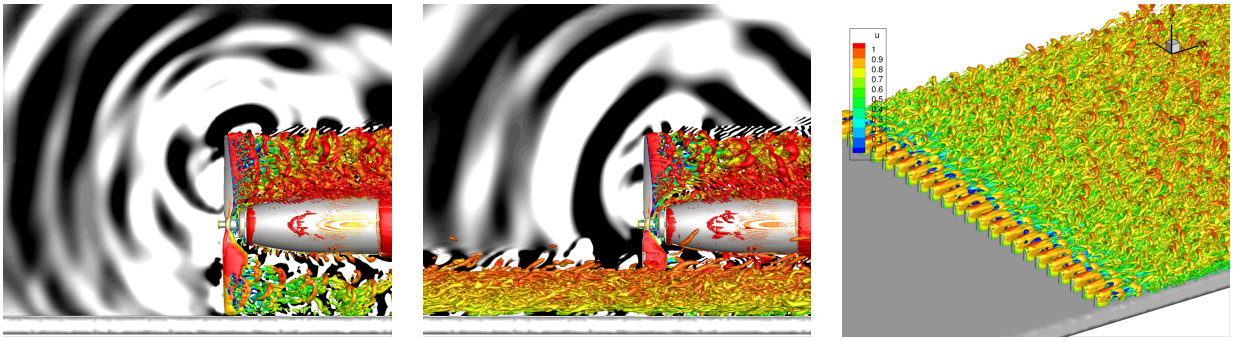

Figure 6: Instantaneous view of the flow for the ZDES mode 2 (left) and mode 3 (center) simulations. Iso-Q surfaces colored by the streamwise velocity value. Gray scale: dilatation field. Right: focus on the tripping device at the inflow of the computational domain for the ZDES mode 3 simulation.

Overall, it has been observed that the turbulent fluctuations from the boundary layer have a much lower intensity than the ones in the wakes of the blades. However, their influence on the wake development downstream of the immersed blade is not negligible. These differences seem to also influence the acoustic radiation (tonal peaks and directivity), by inhibiting the acoustic interferences between the two blades. This must be confirmed by additional investigations, that will be performed in future works. The experimental results were unfortunately not yet available in post-processed form when writing this report. Therefore, only a short comparison could be made between the simulations and the measurements, using preliminary hot-wire measurements carried out in the flat plate boundary layer, in the absence of

propeller. On the basis of this first analysis, it turns out that there exists a mismatch between the overall turbulence intensity in the boundary layer. This can probably be due to the tripping device used in the experiment that prevents the boundary layer to return sufficiently fast to a canonical state. A more thorough comparison with the recent measurements from UTWE will be performed in the next months.

3.2.1 Dissemination (Publications + link ZENODO)

The numerical results have been uploaded in the following Zenodo repository: `https://zenodo.org/record/8322105`.

3.3 ONERA contribution to configuration A2-ducted

3.3.1 Introduction

The configuration A2-ducted is similar to the configuration A2, except that the propeller is replaced by a ducted propeller, whose design is based on the X-22 propeller. This configuration was not planned at the beginning of ENODISE project and has been added due to an interest from ONERA side (with a contribution limited to numerical simulations). Despite the additional amount of work it required, UBRI kindly agreed to include the configuration in their test matrix to provide related experimental data. The presence of the duct slightly increases the complexity of this configuration (with respect to the A2-configuration) and makes it closer to turbofan architectures.

3.3.2 Context and objectives

The main objectives of ONERA numerical predictions on A2-ducted configuration are 1/ to evaluate the effects of boundary layer ingestion on aerodynamic and acoustic performances of a generic ducted propeller; 2/ to provide a numerical database that could be used for developing analytical or data-driven models dedicated to the assessment of such effects; and 3/ to validate the employed numerical methodology against UBRI experimental data.

3.3.3 Main achievements

Numerical simulations have been realized using the lattice Boltzmann solver *ProlB* (`http://www.prolb-cfd.com/`) for the isolated ducted propeller (without the S-plate) and for the installed ducted propeller (with the S-plate) at various rotational speeds. These simulations allow for a direct noise assessment of the setup thanks to the low-dissipative characteristics of the method. One illustrative result is given in Fig. 7 where the Power Spectral Density (PSD) on the 90° microphone of the side arc of the experimental setup is shown for each computed case. The effect of increased rotation speed on the broadband noise is moderate and is mainly observed at low frequencies, while the ingested separated flow has a dramatic impact with a significant increase of the levels over the whole spectrum.

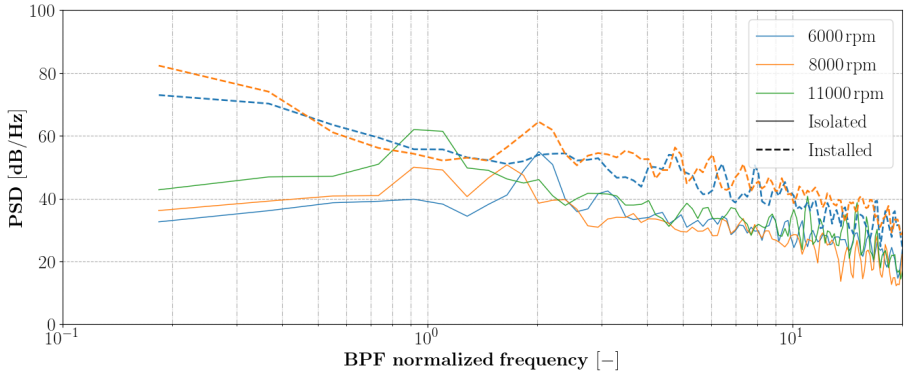

Figure 7: PSD on the 90° microphone of the side arc of the experimental setup for each computed case.

3.3.4 Lessons learnt

This work has shown an important increase of broadband noise when a boundary layer is ingested. It should be kept in mind that this noise increase is directly linked to the predicted ingested flow profile which seems to be different from the experimental one after first qualitative comparisons. This shows how such profiles are hard to capture with blind simulations, especially with the current method that uses an octree mesh and wall laws. An update of installed propeller simulations could be envisaged depending on the forthcoming more detailed comparisons with experimental data.

3.3.5 Dissemination

The results of the performed simulations have been uploaded on a dedicated Zenodo repository (`https://doi.org/10.5281/zenodo.8280145`).

3.4 UR3 contribution to configuration A1

3.4.1 Context and objectives

The UR3 activity regarded the analysis of the experimental data provided by the UBRI research group and related to the configuration A1. In this research, two distinct boundary layer thicknesses were taken into account, with an analysis comparing the performance of 3-bladed and 5-bladed propellers. The freestream velocity maintained a constant value of 20 m/s, and the chosen advance ratio (J) spanned the range of [0.56, 0.98]. The analyses included information such as the Overall Sound Pressure Level, PSD maps, Spectra Scaling and a preliminary wavelet analysis. These metrics are provided for four different scenarios, each involving variations in the number of blades and boundary layer thickness.

3.4.2 Main achievements

- Haystacking more severe for low-number blade configurations and low advance ratios;
- Haystacking significant for $BPF \geq 2$;
- Installation effects more significant for small propeller-surface distances, specifically: (i) amplification of high BPFs when the surface is installed close to the propeller, (ii) increase of the broadband component for close-coupled configurations;

3.4.3 Dissemination (Publications + link ZENODO)

Michele Falsi, Ismaeel Zaman, Matteo Mancinelli, Stefano Meloni, Roberto Camussi, Bin Zang, Mahdi Azarpeyvand . Experimental investigation of the noise emitted by two different propellers ingesting a planar boundary layer. AIDAA 2023, PADOVA
Link ZENODO: `https://zenodo.org/records/8358762`

4 Summary of the results obtained for the configurations B: distributed pylon- and control surface-mounted propulsion systems

4.1 VKI contribution to configuration B1

4.1.1 Context and objectives

Predicting noise levels and describing the mechanisms that cause noise to be produced when a wing is present behind a propeller were the objectives of this study. The geometry was simulated using numerical methods that allow for minimal computational resources for a geometry corresponding to configuration B1 of the ENODISE project. This was accomplished by simulating different geometries using a hybrid uRANS-FEM approach. This technique makes it easier to analyze how different geometric features affect the flow and makes it possible to distinguish between *aerodynamic installation effects* and *acoustic installation effects*. The drawback is that only tonal loading noise has a solution.

4.1.2 Main achievements

The study concludes that wing noise is a crucial source of noise in a propeller-wing configuration, at least for the analyzed advance ratio condition. In the horizontal plane, both the wing and the blade sources have approximately the same peak SPL, but their directivities are markedly different. While propeller noise is primarily in the plane of the rotor, wing noise dominates in the perpendicular direction, which aligns with the expected dominant orientation of the wing's normal vectors.

The presence of the wing had a minimal impact on the steady aerodynamics of the propeller, with only a slight increase in thrust observed. This is attributed to the large distance between the rotor plane and the wing's leading edge. Contrarily, the wing's presence caused a significant increase in the first BLHs of the thrust, which suggests may they be primarily associated with the upwash mean velocity induced by the lifting wing, affecting the inflow on the propeller plane.

The aerodynamic installation resulted in a change in noise directivity at the first two BPFHs, with a notable increase in noise below the wing and in the plane of rotation. The acoustic installation had a slightly lower effect but increased the noise in almost every direction, with the exception of a 20 dB increase in the axial direction due to leading-edge scattering.

Especially in downward radiation directions, the wing, subjected to the incoming wakes of the propeller blades, appears to be the most significant source of noise. In the vertical plane, the noise from the wing dominates the propeller noise by more than 20 dB in some directions. Despite the Doppler amplification applying to the propeller blade, the wing's acoustic non-compactness makes it a more efficient acoustic source.

4.1.3 Lessons learned

These findings underscore the complexity of the interactions in a tractor propeller-wing configuration and the need to consider both aerodynamic and acoustic factors in design and analysis. Additionally, the significant noise contribution from the wing, not just the propeller should be analyzed for UAM vehicles. The research also underscores the value of quick computational methods in addressing these challenges, pointing towards the need for further research on various aircraft configurations to reduce noise pollution in urban areas.

4.1.4 Dissemination (Publications + link ZENODO)

The simulation data can be found at `https://zenodo.org/records/8306236` in the form of *CGNS* files for the sources pressures over the geometry. The full results are published at the DOI: `https://doi.org/10.2514/6.2023-4056`.

4.2 SISW contribution to configuration B1

Siemens Industry Software (SISW) studied numerically the six-blade pylon-mounted XPROPS propeller of the experiment carried out at Ecole Centrale Lyon (ECL) in the context of ENODISE project. The propeller operates at a rotational speed of 7000 rpm. Two operating conditions (without and with upstream flow) have been considered corresponding to advance ratios J of 0 and 0.928, respectively. More details about these configurations can be found in ECL experimental database available in Zenodo (`https://zenodo.org/record/7925336`). A view of the propeller and its support is provided in Fig. 8.

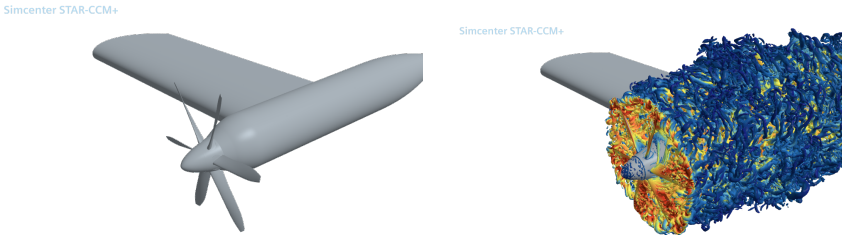

Figure 8: Representation of (a) the pylon-mounted XPROPS propeller and (b) Q-criterion isocontours colored by velocity magnitude obtained from DES at $J = 0$.

4.2.1 Main achievements

The main objectives of this study have been to examine the effect of the pylon on the flow development and acoustic field, and to generate high-fidelity numerical results in order to assess the performance of the low-fidelity Amiet-based models developed by SISW and the von Kármán Institute in ENODISE Work Package 2. For this purpose, the numerical strategy adopted by SISW for tonal and broadband noise predictions consists of a two-step approach. In the first step, three-dimensional incompressible unsteady CFD simulations (Large-Eddy Simulation (LES) or Detached-Eddy Simulation(DES)) of the pylon-mounted propeller configuration have been performed using commercial software Simcenter STAR-CCM+ [10] in order to compute the instantaneous pressure field on the propeller blades and on the pylon. For illustration purposes, an instantaneous snapshot of the flow simulation carried out for $J = 0$ is provided in Fig. 8. In a second step, high-order Finite-Element (FE) acoustic simulations [11, 12] have been performed in Simcenter 3D [13] to compute noise predictions accounting for installation effects. Numerical results have been successfully compared to ECL experimental data.

4.2.2 Lessons learnt

This study demonstrated that the presence of the pylon affects the flow development (potential flow effects) and contributes to noise in the presence of flight stream flow ($J = 0.928$). This observation argues in favour of accounting for the effect of the pylon in the analytical and numerical aeroacoustic models. The present numerical approach, based on the combination of incompressible high-fidelity CFD computations with FE acoustic simulations, has proven to be an efficient way to get reliable acoustic predictions at a reasonable computational cost.

4.2.3 Dissemination

Numerical results, including propeller performance as well as tonal and broadband acoustic predictions have been published in Zenodo (`https://zenodo.org/record/8176756`). One conference paper and a journal article are under preparation.

4.3 ONERA contribution to configuration B1

4.3.1 Context and objectives

A 3 steps-chaining method has been evaluated to predict the installation effects of the 3-puller-propeller configuration B1 with a wing profile downstream on the emitted tonal-noise and its directivity. The in-house CONCERTO chain, composed of the PUMA code (lifting-line method), the KIM code (a Ffowcs-Williams-Hawkings based-method), and finally the BEMUSE code (Boundary Element method) is employed to evaluate the influence of the blades phase angles and of the wing profile on the tonal-noise and its directivity. The present numerical results are aimed to be compared to the TU Delft experimental campaign datas operated in WP3 (D3.4).

4.3.2 Main achievements

This work allowed us to apply the CONCERTO code to a 3 puller-propeller configuration: in particular, it shows that aerodynamics interactions between the propellers can be taken into account in the performances predictions by the PUMA code. Then, it shows that the incident pressure of the wing profile surface coming from the total contribution can be taken into account and predicted by the KIM code. Finally, this work underlines the capability of this methodology to take into account the phase-angle into the total noise predictions.

4.3.3 Lessons learnt

This methodology can be further compared to TUDelft Experimental results (D3.4) and tested on other configurations to precise the methodology capability to predict the installation effects.

4.3.4 Dissemination

The ONERA database contains numerical results about aerodynamic performances (thrust, torque and efficiency). It also includes pressure and sound pressure levels on the arcs microphones positions of TUD experimental configuration. Datas are stored in .dat and .plt format files. These latter are available on the Zenodo repository under the following link: https://zenodo.org/record/8308001.

4.4 DLR contribution to configurations B1

4.4.1 Context and objectives

The aim of DLR research was to improve the understanding of noise emissions from distributed propulsion systems using a rapid prediction method based on analytical models. The insights gained hold potential for optimising such configurations, which are important for the development of quieter and more efficient flying vehicles, especially in the context of regional and urban air mobility. The aim was to investigate the role of purely acoustic interference and its influence on the tonal noise radiation of multirotor configurations.

4.4.2 Main achievements

A method using an analytical model able to quantify the acoustic emission associated with such a configuration was developed. Initially, the pressure distribution around blade profiles was computed using XFOIL (similar approach as for configuration A). The resulting polar diagrams were used by the Blade Element Momentum Theory to determine the propeller aerodynamic performance, the mutual aerodynamic interaction between propellers was neglected. The accuracy of this approach was validated with the experimental data collected at TU Delft as can be seen in Fig. 9.

Building upon the aerodynamic results, the acoustic emission was calculated using the acoustic analogy, as described in Ref. [14]. This approach enabled to calculate the rotor self-tones due to steady lift, drag, and thickness, as well as the interaction noise arising through the interaction of the rotor wakes with the wing. Interference effects between individual noise sources were obtained using an extension of

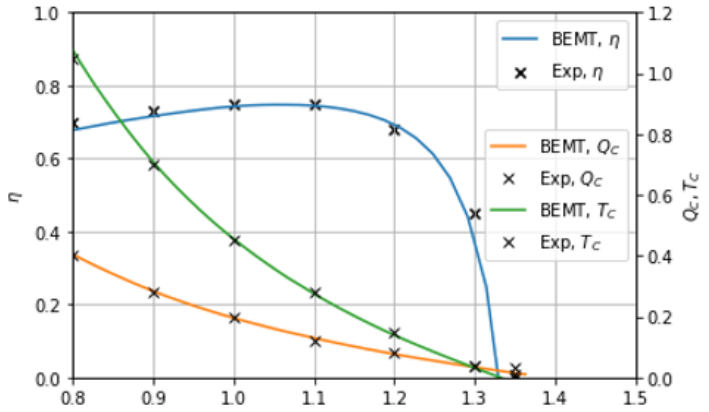

Figure 9: For the X-PROP-S propeller, comparison of the performance parameters (thrust and torque coefficients, efficiency) obtained with the BEMT approach of DLR and the measurements performed by TUD.

the method described in Ref. [15]. The initial prediction efforts were devoted to the acoustic emission from the reference configuration. Far from the simple case, the results (reproduced in Figure 10) revealed the complexity of the directivity patterns. They also showed that the interaction between the rotor wakes and the wing could be the dominant noise mechanism, especially in the axis of the flow ($\Psi = 0°/180°$).

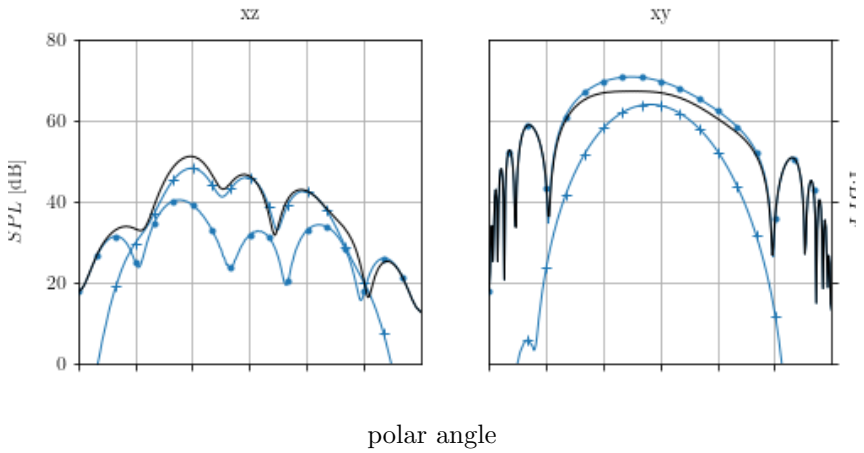

Figure 10: SPL directivity calculated for the three propellers+wing configuration at 1.5 m distance; co-rotation, $\Delta\Phi = 0°$, $J = 0.8$; (o) rotor–wing interaction, (+) rotor selfnoise, (black solid line) total contribution.

4.4.3 Lessons learned

The study was concluded with an important result: The purely acoustic interference between rotors and rotors and blades has a drastic influence on the noise radiation of multirotor configurations. This must be taken into account when choosing the relative position between the rotor and the rotor blades, as the interference effects strongly depend on this choice.

For small distance between open rotors, that is, small tip-to-tip gap, the aerodynamic interaction between the blades becomes important as shown by the experiments, and therefore, it should be included in the models. Including this effect in the analytical approach will require new models.

The study also showed that the interaction between rotor and wing is a very strong source of tonal

noise, the importance of which increases with the harmonic order of the BPF. This result is consistent with previous studies, but needs further confirmation.

4.4.4 Dissemination (Publications + link ZENODO)

The results regarding the calculation of the reference configuration were presented by Lade et Guérin [16], in Berlin (Germany).

The results were uploaded on Zenodo repository and can be accessed using this link: `https://zenodo.org/record/8112891`.

4.5 RWTH contribution to configuration B1

4.5.1 Context and objectives

The main object of this work is to perform wall-resolved Large eddy simulations (LES) coupled with a CAA solver for the prediction of the aerodynamic and acoustic flow field of the propeller-pylon interaction configuration. The test setup is the ENODISE-B1 configuration with an incoming flow velocity of $U_\infty = 30$ m/s, an advance ratio of $J = 0.8$, and an angle of attack of $AoA = 2°$. The acquired numerical results will be cross-validated against the experiments conducted by TUDelft and serve as a reference database for future analysis and optimization. A preliminary analysis of the results has indicated the potential noise sources due to the impingement of the propeller tip vortex on the leading edge of the wing, which can provide guidance for the subsequent design of noise mitigation treatments on the wing surface.

4.5.2 Main achievements

Large-eddy simulations of the ENODISE-B1 configuration are conducted using the multiphysics flow solver m-AIA of RWTH. The Navier-Stokes equations are solved by a finite volume (FV) solver at second-order accuracy in time and space to perform wall-resolved LES of the turbulent flow field. A level-set solver based on the kinematic motion level-set approach is employed to track the rotating geometry of the propeller blades, providing information about the surface location for solution adaptive mesh refinement (AMR) during the simulation run. A postprocessing module is integrated into the simulation workflow to conduct time averaging or time-series data sampling. For the far-field noise, the Ffowcs-Williams and Hawkings (FW-H) method formulated in the frequency domain is used to predict the pressure signals at far-field observer positions. The flow field simulation has been performed for over 7 propeller rotations and the postprocessing module has been run for over 3 propeller rotations.

For the aerodynamic results, the vortex structures in the flow field denoted by Q-Criterion are shown in Fig. 11. The tip vortices impinge on the leading edge of the wing and break down while traveling around the wing. Regarding cross-validation, the predicted (a) propeller thrust coefficient Tc, (b) distribution of pressure coefficient Cp on the airfoil surface, and (c) the distribution of the total pressure coefficient CpT two chord length downstream of the wing are in good agreement with the experimental data from TUDelft, demonstrating the accuracy of the present method in predicting the turbulent flow field. Pressure fluctuation on the wing leading edge is shown in Fig. 12. Regions of high-pressure fluctuation are found where the propeller tip vortex impinges the leading edge of the wing, resulting in unsteady loads on the wing and interaction noise. These results could suggest the locations for future noise mitigation treatments on the wing surface.

For the aeroacoustic results, the power spectral density (PSD) of the far-field noise predicted by the FW-H method has been compared with the wind tunnel measurements from TUDelft. The FW-H predictions have good consistency with the wind tunnel measurement in the high-frequency broadband range. Tonal frequencies related to the blade passing frequency (BPF) are also captured correctly. However, the amplitude of low-frequency tonal noise deviates from the experimental results. There are two possible reasons for this difference. On one hand, the acoustic results have not yet fully converged due to the small number of simulated revolutions of the propellers, which will be addressed in future updates. On the other hand, the simulation employed the periodic boundary conditions to model an infinitely long array of propellers, which differs somewhat from the TUDelft experimental setup with a

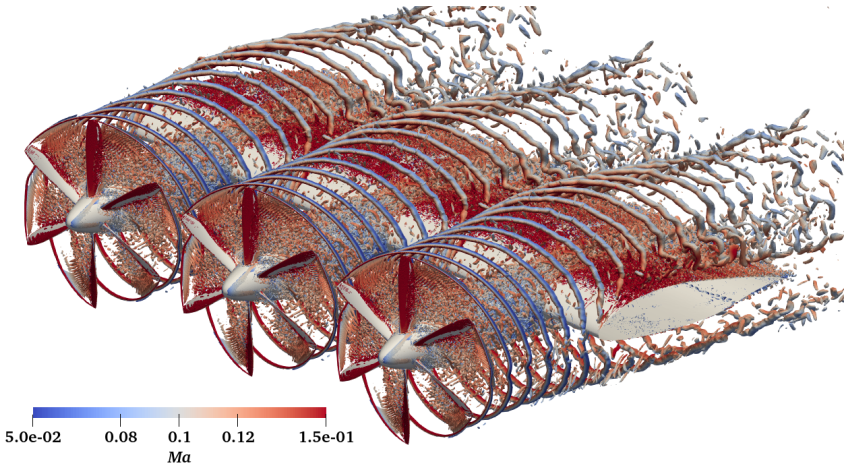

Figure 11: Vortex structures denoted by Q-Criterion

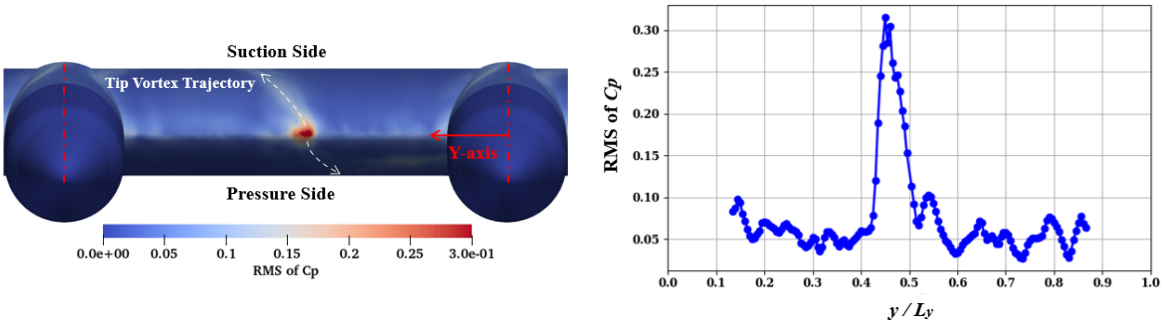

Figure 12: Pressure fluctuation on the wing surface

three-propeller layout. This geometrical discrepancy could lead to a certain degree of difference in the tonal noise amplitude.

4.5.3 Lessons learned

The cross-validation with the experimental data has demonstrated the capability of the present method in the prediction of the turbulent flow field and far-field noise level of the propeller-pylon interaction configurations. The acquired high-resolution numerical results could be used as a reference database for future analysis and optimization. Regions of high-pressure fluctuation on the leading edge of the wing due to the impingement of the propeller tip vortex present a potential location for noise mitigation treatments, such as porous inserts and serrations, which will be investigated in a further work package.

4.5.4 Dissemination

The numerical results for the ENODISE-B1 configuration are available on the Zenodo repository under the following link: `https://doi.org/10.5281/zenodo.8320292`. The data set contains the time-averaged flow field results predicted by a high-resolution LES and the far-field noise prediction determined by the FW-H method. One conference paper and a journal article are under preparation.

4.6 ECL contribution to configuration B2

4.6.1 Context and objectives

Apply analytical methods to the selected propeller-wing configurations accounting for complex installation effects, to assess their ability to ensure satisfactory prediction accuracy with an acceptable computational cost, before being used in optimization platforms.

4.6.2 Main achievements

A global analytical prediction scheme of propeller tonal noise was developed, by combining three analytical models, one for steady loading-noise sources, one for unsteady loading-noise sources caused by inflow distortions, and one for the scattering of modal sources by a truncated half-plane. It is dedicated to typical wing-propeller arrangements corresponding to configuration B2 in the project, involving two side-by-side propellers installed in the rear part of a wing. The modeling approach is divided into two steps. In the first step, the blade forces acting as equivalent dipoles are determined. Steady forces are inferred from the blade-element momentum theory. Lift fluctuations responsible for unsteady-loading noise are determined by Sears' theory from stationary velocity distortions computed by Siemens. Equivalent circular arrays of stationary phased dipoles called source-modes are also introduced. In the second step, the radiation of source-modes is calculated at any point, including sound scattering by the wing, via the use of the half-plane Green's function, modified to account for finite chord. Outputs of the model are tonal noise levels and associated three-dimensional directivity diagrams. Despite its simplifications, the model allows the quantification of sound masking and diffraction effects by the wing. Typical simulated sound fields are shown in Fig. 13, illustrating the crucial effect of unsteady noise sources, associated with the presence of the pylons. Fig. 14 displays the effect of propeller positioning close to the wing trailing edge.

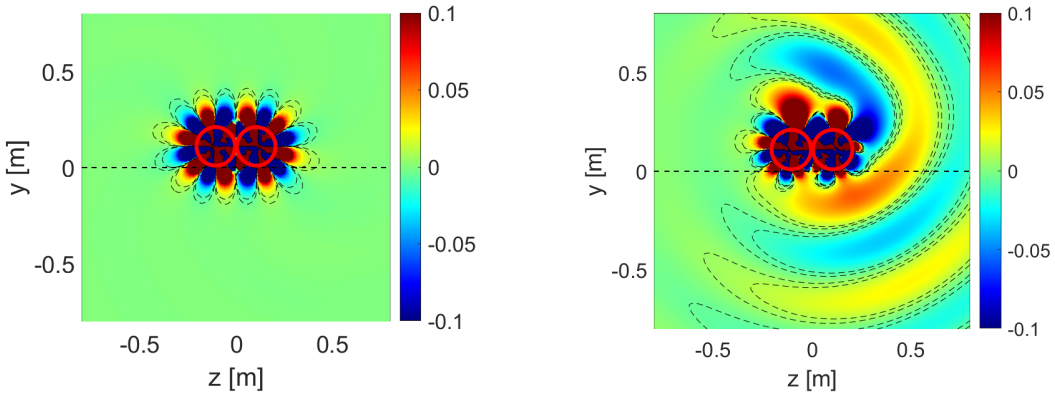

Steady-loading noise sources

Unsteady-loading noise sources

Figure 13: Instantaneous free-field sound-pressure maps for co-rotating propellers and different sources. The propellers are featured by the red circles and the removed-wing position by the dashed black line.

4.6.3 Lessons learned

Analytical predictions of sound scattering of propeller noise by the trailing edge of a wing highlighted regimes of amplification and masking of the tonal noise when blade tips operate at acoustically-compact distance from the TE and over the wing, respectively. This effect was also observed in the experiments. Therefore, the analytical model appears as a good candidate for fast and accurate calculations within the scope of parametric studies or optimization algorithms. Analytical modeling can be achieved with only an approximate and incomplete description of the addressed system, at the early design stage.

Edge scattering in the amplification regime is able to redefine the ranking of sound generating mechanisms, especially the relative contribution of steady-loading noise.

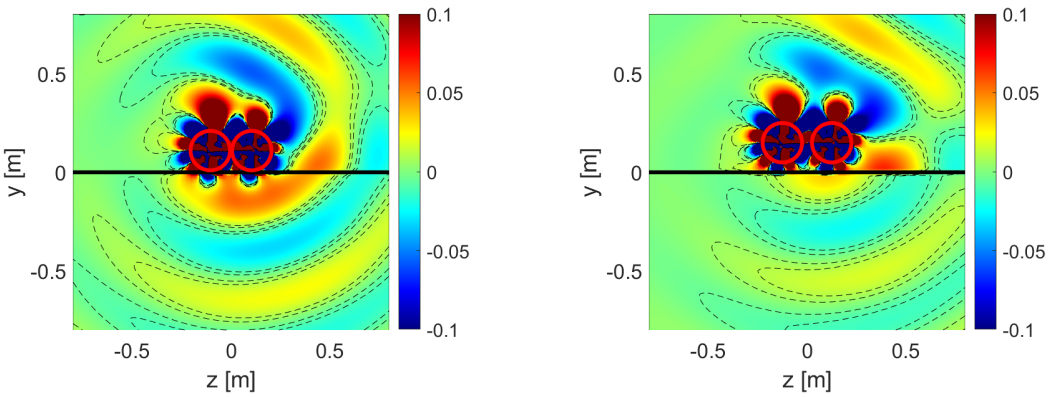

Propellers close to the TE

Propellers over the wing

Figure 14: Instantaneous scattered-field sound-pressure maps for steady and unsteady-loading noise sources in the case of co-rotating propellers. The propellers are featured by the red circles and the wing is shown in black.

4.6.4 Dissemination (Publications + link ZENODO)

- Conference paper: **Acevedo-Giraldo, D.**, Roger, M., Jacob, M. C., & Beriot, H. (2022). Analytical study of the aerodynamic noise emitted by distributed electric propulsion systems. In 28th AIAA/CEAS Aeroacoustics Conference 2022 (p. 2830).
  `https://doi.org/10.2514/6.2022-2830`
- Database ZENODO: `https://zenodo.org/records/8182284`

4.7 ONERA contribution to configuration B2 - Auralization

4.7.1 Context and objectives

An auralization on the B2 configuration has been performed. To that purpose the in-house noise synthesis tool FLAURA was used.
This work had two objectives: one, to assess the audible impact of phase shift and propeller spacing on auralized sounds; the second, the comparison on an auditory level of propeller noise measurements and numerical simulation results. ECL measurement data (https://zenodo.org/record/7925336) and Siemens numerical simulations (https://zenodo.org/record/8176756) were used and partially compared.

4.7.2 Main achievements

First, it was verified that the synthesis procedure does not alter the sound signals.
In a second step, by comparing different two-propeller configurations, the impact of varying phase shift and/or spacing between the propellers was assessed. It appears that tonal noise amplitude, which is sensitive to phase information, is indeed modified by spacing and phase variations, however the sound does not perceptibly change. These amplitude changes might be partially masked by the high level motor harmonics.
Then, a comparison was done for flow and no flow one propeller configurations between measurement data and numerical results. For the no flow configuration measured motor noise was added to the noise simulation. Since the simulation has only a range of 117 Hz to 3500 Hz, below and above the signal is composed of motor noise only. The auralized wav file sounds very different to the measurement. Indeed, the whole aspect of the sound is different, but one can also hear a high frequency pitch that might come from the motor but is not present in the propeller noise measurement.
For the flow configuration, motor and background noise were added to the numerical result. The auralized

sound only emerges from the background and the motor noise between approximately 100 Hz and 200 Hz, leading to a sound file where one can barely hear propeller noise.

4.7.3 Lessons learnt

During the study of the impact of phase shift and spacing on the audible sound, it appears that auralizations show certain shortcomings. A difference is heard when comparing measured 2 propeller configurations with auralizations where a single propeller is auralized, propagated to the receiver and summed with another propeller signal (taking into account the phase shift). The audible difference seems to come from the motor harmonics that are not treated as tonal noise in the auralization process, and therefore keep a random phase.
When comparing numerical simulation results to experimental data, it appears that motor and background noise have a significant contribution to the total sound, implying that the propeller noise simulation needs to cover a large frequency range to not be masked by it. Furthermore, in this study motor noise was only measured for no flow configuration, but added to flow and no flow noise simulations, making the flow configuration artificially focused on the overestimated motor noise.

4.7.4 Dissemination

Auralized signals are stored as *wav* files on the Zenodo depository under the following link: `https://zenodo.org/record/8321964`.

5 Summary of the results obtained for the configurations C: multi-rotor propulsion systems

5.1 VKI & SISW contribution to configuration C

5.1.1 Context and objectives

The goal was to predict noise levels and outline the mechanisms behind noise production in open contra-rotating propellers (CRP) and shrouded contra-rotating propellers (S-CRP), specific to configuration C of the ENODISE project, through the use of numerical techniques that allow for reasonable computational resources. This was achieved by utilizing a hybrid uRANS-FEM method for the simulation of various geometries. This method facilitates the analysis of how various geometric aspects influence the flow and enables the differentiation between *aerodynamic installation effects* and *acoustic installation effects*. The limitation is that a solution is only provided for tonal loading noise.

5.1.2 Main achievements

The aerodynamic methodology employed yields results with a reasonable degree of accuracy. For the validated CRP setup, the calculated average thrust deviates by less than 5% from experimental findings and is consistent even as mesh cell density increases. The velocity of the wake behind the propeller shows a close correlation with the experimental hotwire studies. The acoustic methodology presents a decent correlation with the experimental data at the tonal peaks, suggesting that the tonal noise significantly influences the overall noise profile. The approach proves particularly proficient in predicting lower harmonics across all configurations and higher harmonics for setups with periodic loading. However, its performance falters when loading noise isn't the prevailing factor.

In analyzing the open contra-rotating propeller setup, there is an increase in blade loading at frequencies corresponding to the interaction frequency (blade overlap frequency). This interaction stems from the propellers' mutual potential field interaction noticed from their symmetrical results in their performance. Individually, each blade's performance decreases, with the rear propeller especially impacted in its inner section by the wake generated by the leading propeller.

Acoustic emissions are predominantly influenced by the unsteady conditions introduced by interaction tones, while the steady loading only experiences minimal effects from reduced mean thrust. Tones at other harmonics of the BPF, due to interaction tones, are shown to exist as predicted by analytical formulas.

The addition of a shroud reduced the system's overall performance at the same RPM settings. The shroud caused separation on its inner surface, negatively affecting both propellers. Although the impact varied based on propeller location, overall thrust performance became roughly equal. The shroud itself contributed about one-third of the total thrust from its leading edge.

The changes in aerodynamic flow and performance primarily affected the steady loading of the propellers, causing small impacts on noise at lower frequencies. Additionally, when examining acoustic emissions, it was found that they depended on the propellers' proximity to the shroud's leading edge. The leading edge scattering redirected noise in different directions, resulting in more uniform noise distribution, particularly increasing noise in the rotor plane, which was initially low.

5.1.3 Lessons learned

The analysis has yielded important insights. Firstly, the hybrid methodology used proved reliable, accurately predicting thrust and wake velocity for the CRP setup, albeit with limitations when loading noise is not predominant. Secondly, understanding the interaction frequency is crucial in open contra-rotating propeller setups, as it increases blade loading due to mutual potential field interaction between propellers. Lastly, the addition of a shroud significantly impacted system performance, affecting thrust and noise distribution. Recognizing the shroud's influence is vital for assessing overall performance and noise emissions.

These findings emphasize the need for a comprehensive analysis, considering propeller configurations and additional components like shrouds when evaluating such systems. Future studies should seek to

analyze blade interactions, optimize shroud design, and address the complex interdependencies of system parameters. Additional deep dives into the mechanism that generates the increase in noise due to the shroud's acoustic presence are warranted. These studies will advance our understanding of S-CRPs and their applicability in real-world UAM scenarios.

5.1.4 Dissemination (Publications + link ZENODO)

The simulation data can be found at `https://zenodo.org/records/8305812` in the form of *CGNS* files for the sources pressures over the geometry and *CSV* files for the directivities resulting from the acoustic methodology.

5.2 ECL contribution to configuration C

5.2.1 Context and objectives

ECL developed and applied an analytical approach applicable at the early design stage for contra-rotating systems, when too many unspecified details forbid the use of, typically, accurate numerical flow simulation. This is dedicated to repeated fast calculations for parametric studies and optimization algorithms.

5.2.2 Main achievements

Main results were deduced from a far-field expression of the tonal noise generated by the rear rotor because of impinging wakes from the front rotor, referred to as wake-interaction rotor-rotor noise. This includes steady-loading noise and unsteady-loading noise, the sources of which are the constant and periodic parts of the blade forces, respectively. The former is predicted from a simplified iterative version of the Blade-Element Momentum Theory, considering two coupled co-axial rotor discs. The latter is predicted from approximate fluctuating forces, based on realistic wake and tip-vortex models for trajectories and velocity deficits, on the one hand, and on classical Sears' linearized unsteady-aerodynamic theory, on the other hand. The blades are split into a couple of segments acting as equivalent rotating dipoles; the strength of the dipoles is defined by the Fourier coefficients of the blade forces, called blade-loading harmonics. Calculation are made in free field, ignoring duct effects. All parameters can be easily changed for inspection of the related effects, typically the rotating speeds, rotor-rotor distance, blade counts and so on. Symmetric systems (same blade numbers on both rotors and identical rotating speeds in opposite directions) are known to generate tones at harmonics of the common blade-passing frequency. Asymmetric systems, addressed here with same rotation speed but different blade numbers, generate combination tones at all linear combinations of multiples of the two blade-passing frequencies.

Near-field calculations could be performed from the same basic model, by associating source-modes to each blade-loading harmonic. Furthermore, the potential-interaction noise emitted by the front rotor, because of the potential flow distortion around the rear rotor, could be simulated in the same way, provided that a description of the potential field is available.

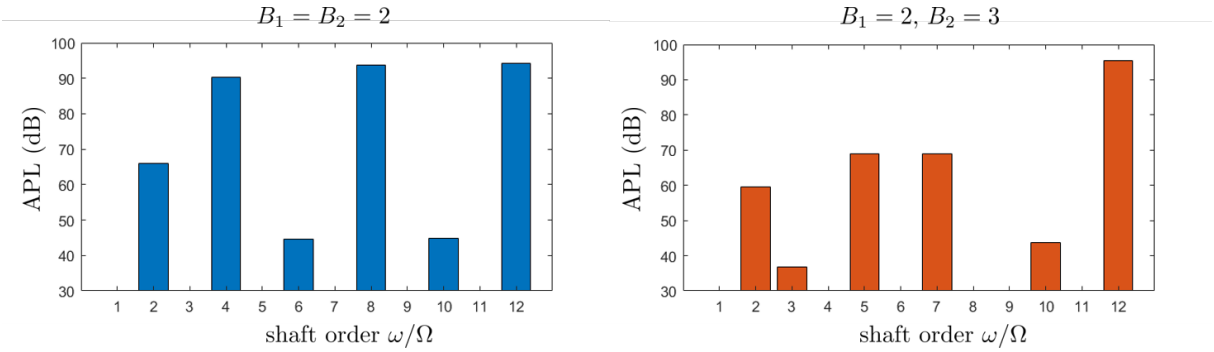

Figure 15: Sound-power bar-graphs of the wake-interaction tonal noise, for the symmetric system $B_1 = B_2 = 2$ (left) and the system $B_1 = 2$, $B_2 = 3$ (right), in conditions of expected similar thrust.

Key results comparing power spectra of the tonal noise in the case of blade numbers B_1 and B_2 on the front and rear rotors both equal to 2, corresponding to the VKI experiment, and in the hypothetical case where $B_1 = 2$ and $B_2 = 3$, are plotted in Fig. 15. The decibel scale emphasizes on the dominant tones. The results suggest that the arrangement $B_1 = 2$, $B_2 = 3$ should globally produce a lower noise, even if it contains all possible harmonics of the common rotational frequency. Furthermore, the ranking of tonal levels in the symmetric case has been found in good qualitative agreement with measurements performed by the VKI. It is worth noting that the presently reported 'blind' predictions have been made ignoring details of the VKI computations, in order to demonstrate feasibility.

5.2.3 Lessons learned

Simplified analytical models of contra-rotating systems can be run at very low cost at the early-design stage, and provide realistic acoustic results, despite the lack of accurate flow information. Analytical modeling appears as a reliable low-noise design tool. The preliminary tests indicate that asymmetric systems involving different blade numbers on both rotors could bring some benefit.

5.2.4 Dissemination (Publications + link ZENODO)

The advances have been presented recently in:

Roger, M., Preliminary Analytical Modeling of the Tonal Noise of Co-Axial Contrarotating Rotors for Drone Propulsion, Feri Farassat Aeroacoustic Symposium, Capri 2023, Italy.

The simulation data can be found *via* the link `https://zenodo.org/record/8301188`.

5.3 ONERA contribution to configuration C

5.3.1 Context and objectives

The objective is to numerically predict the noise emitted by contra-rotating and co-axial propellers placed in a shroud corresponding to the configuration C of the ENODISE project. High fidelity simulations are indented to provide further assessment of the noise source mechanisms and supplement fast prediction methods.

5.3.2 Main achievements

Simulations using a Lattice Boltzmann Method (LBM) have been performed with the ProLB code [17]. Taking advantage of the low dissipation/dispersion of this method, the noise is directly computed and extracted from the CFD simulations. Flow field extractions have also been made. The effect of the duct will be studied by considering cases with and without the shroud. A single operating condition is considered with a rotation speed of 6000 RPM and an interstage distance of 3 cm.

The total number of points for the shrouded case is equal to 346 million. A detailed view of the mesh is shown in Figure 16, high mesh density regions are adopted to protect the wake and duct areas as well as the acoustic waves propagation area. To ensure statistical convergence the simulation is run over 12 revolutions over which 7 are used for acoustic post-processing.

Experimental results are only available to the unshrouded case. Consequently, for the time being comparisons with measurements are limited to this configuration.

In terms of thrust, the measurements [18] gives a value of 18.85 N for the complete configuration. The simulation overestimates this value by 0.4 N i-e 2.1%.

Illustrations of the flow structures in Figure 17 show the Q criterion colored by vorticity for both configuration.

Comparisons in terms of noise spectra are proposed in Figure 18 for one microphone placed upstream of the rotor, inclined at 10.6°, and positioned 56 cm away from the rotor axis. Tonal and broadband signals have been obtained thanks to a phase averaging. The global tendency is very well captured. The broadband noise seems to be slightly underestimated while on the other hand the tonal component appears to be a bit overestimated depending on the tones considered.

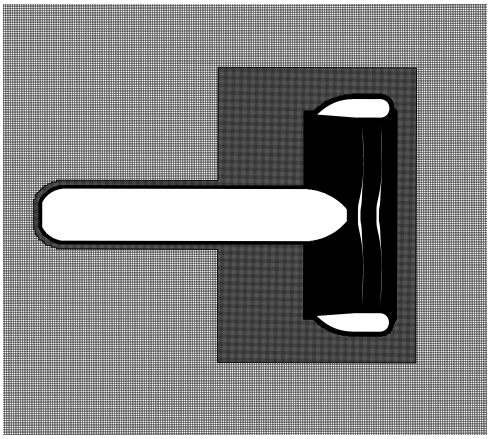

Figure 16: Detailed view of the mesh

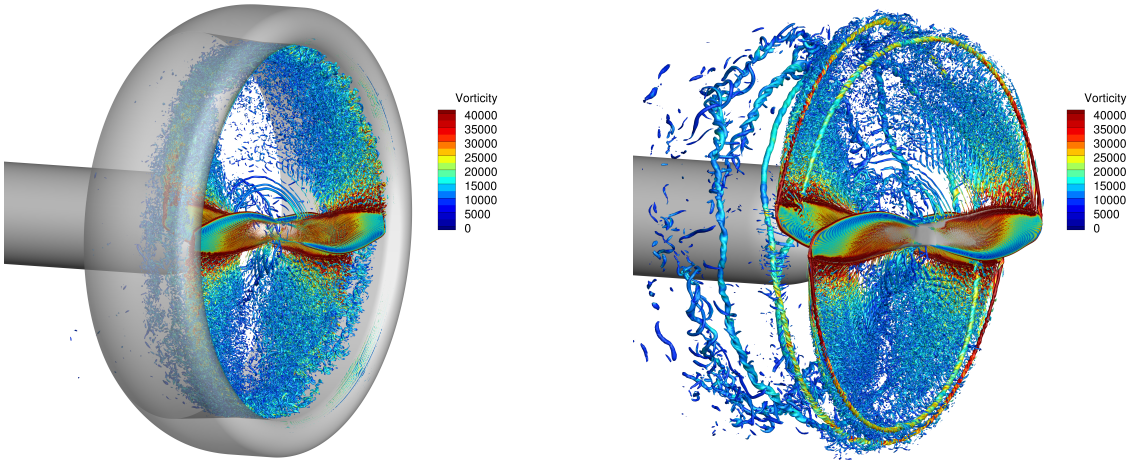

(a) Shrouded case (b) Unshrouded case

Figure 17: Q criterion colored by vorticity

A comparison of the sound directivities with and without shroud are presented in Figure 19. In this figure, 0° corresponds to the upstream direction. The influence of the wake is well visible at 180°. Also, one can observe surprisingly that the shrouded case is louder. This result will need to be confirmed by the experimental results when available.

5.3.3 Lessons learnt

The present simulations have shown that the near field noise generated by a counter-propellers equipped or not with shroud can be directly predicted thanks to the proLB code. A good accuracy has been observed for the unshrouded case for which experimental results are available. This still need to be confirmed for the shrouded configuration.

5.3.4 Dissemination

A numerical database corresponding to those computations has been created in a ZENODO repository with open-access (https://zenodo.org/record/8191815).

Further dissemination as a conference paper is planned when the complete experimental results will be available.

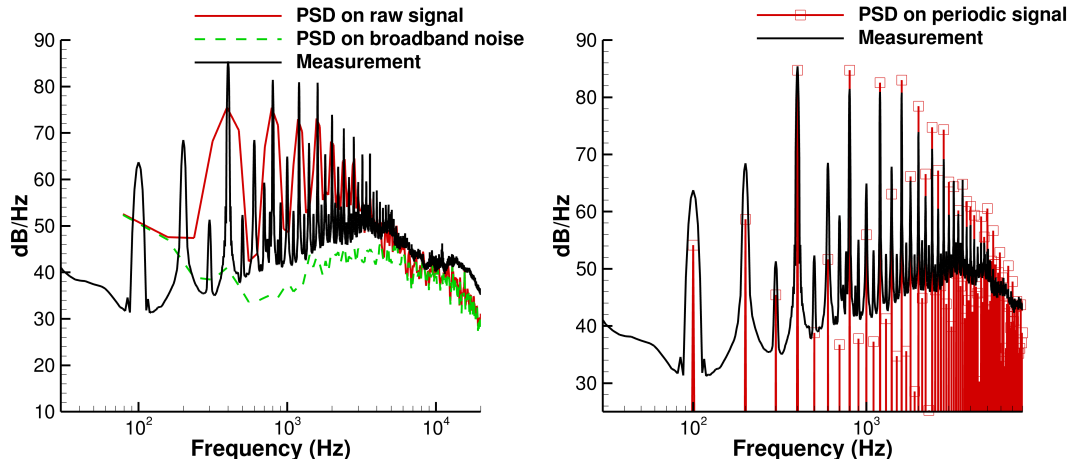

Figure 18: Comparisons of acoustic spectra measured and predicted on the unshrouded configuration.

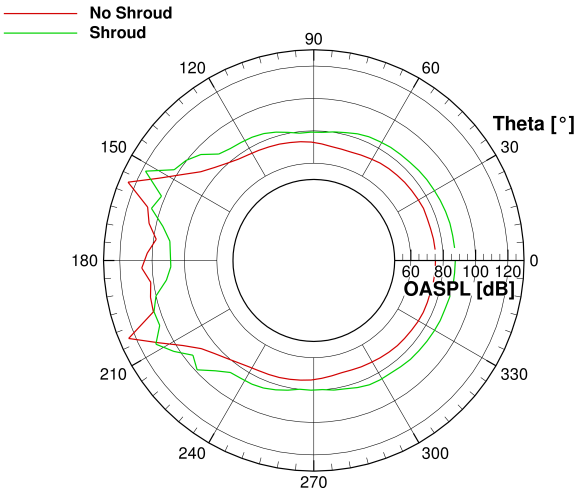

Figure 19: Noise directivity with and without shroud

6 Conclusion

The partners involved in Work Package 4 have demonstrated their capabilities to predict the noise generated by a rotor ingesting a turbulent boundary layer (A), multi-rotor propulsion systems mounted on pylons and control surfaces (B), and contra-rotating rotors (C). Analytical and numerical predictions were provided for aerodynamic (e.g. thrust, torque) and aeroacoustics (far-field noise spectra) datasets, now publicly accessible on Zenodo.

These datasets, along with the associated postprocessing tools, can be utilized to optimize and mitigate propeller installation effects in future.

References

[1] S. Guérin, T. Lade, L. Castelucci, and I. Zaman. Tonal noise emission by a low-mach low-reynolds number propeller ingesting a boundary layer. Prague (CZ), 9-13 June 2023. 29th International Congress on Sound and Vibration.

[2] S. Guérin, T. Lade, L. Castelucci, and I. Zaman. Broadband noise emission by a low-mach low-reynolds number propeller ingesting a boundary layer. Chiba, Greater Tokyo (JP), 23-26 August 2023. Inter.noise.

[3] Zang B. Azarpeyvand M. Zaman, I. and M. Falsi. H2020 enodise: Ubri experimental aeroacoustic database bli configuration a (v.1.0.1) [data set].

[4] S. Deck. Recent improvements in the zonal detached eddy simulation (ZDES) formulation. *Theoretical and Computational Fluid Dynamics*, 26(6):523–550, 2012.

[5] S. Deck, N. Renard, R. Laraufie, and P. Sagaut. Zonal detached eddy simulation (ZDES) of a spatially developing flat plate turbulent boundary layer over the Reynolds number range $3150 \leq Re_\theta \leq 14000$. *Physics of Fluids*, 26(2):025116, 2014.

[6] M. Terracol, M. Satcunanathan, and M. Meinke. ENODISE deliverable D2.9: ZDES solver with wall models. Technical report, ONERA and RWTH, 2022.

[7] S. Deck and N. Renard. Towards an enhanced protection of attached boundary layers in hybrid RANS/LES methods. *Journal of Computational Physics*, 400:108970, 2020.

[8] Steven R Allmaras and Forrester T Johnson. Modifications and clarifications for the implementation of the Spalart-Allmaras turbulence model. In *Seventh international conference on computational fluid dynamics (ICCFD7)*, pages 1–11. Big Island, HI, 2012.

[9] Donald Coles. The law of the wake in the turbulent boundary layer. *Journal of Fluid Mechanics*, 1(2):191–226, 1956.

[10] Siemens Digital Industries Software. Simcenter STAR-CCM+ (version 17.06.007-R8), 2022.

[11] Hadrien Bériot, Albert Prinn, and Gwénaël Gabard. Efficient implementation of high-order finite elements for Helmholtz problems. *International Journal for Numerical Methods in Engineering*, 106(3):213–240, 2016.

[12] Korcan Kucukcoskun and Axel Kierkegaard. Accuracy and advantages of hybrid solutions compared to direct noise calculations for low-speed fan noise. In *FAN2022 Conference*. Universitäts-und Landesbibliothek Darmstadt, 2022.

[13] Siemens Digital Industries Software. Simcenter Nastran Acoustics User's Guide (version 2212), 2023.

[14] A. Moreau and S. Guérin. Similarities of the free-field and in-duct formulations in rotor noise problems. Portland (USA), 5-8 June 2011. 17th AIAA/CEAS Aeroacoustics Conference (32nd AIAA Aeroacoustics Conference).

[15] S. Guérin and D. Tormen. A contribution to the investigation of acoustic interferences in aircraft distributed propulsion. *CEAS Aeronaut J.*, 2023.

[16] T. Lade and S. Guérin. Acoustic interference between three propellers. Berlin (Germany), 22-24 November 2023. DJINN-ENODISE Conference.

[17] CS GROUP. ProLB web site, http://www.prolb-cfd.com.

[18] E. Gallo, J. de Decker, P. Haezebrouck, A. Zarri, and C. Schram. H2020 ENODISE: Experimental dataset of configuration C VKI, https://zenodo.org/record/7966211.